Title

Temporal Dynamics of Human Frontal and Cingulate Neural Activity During Conflict and Cognitive Control

Journal

Cerebral Cortex, 28(11)

ISSN

1047-3211

Authors

Bartoli, Eleonora
Conner, Christopher R
Kadipasaoglu, Cihan M
et al.

Publication Date

2018-11-01

DOI

10.1093/cercor/bhx245

Peer reviewed

Cerebral Cortex, November 2018;28: 3842–3856

doi: 10.1093/cercor/bhx245
Advance Access Publication Date: 28 September 2017
Feature Articles

FEATURE ARTICLES

Temporal Dynamics of Human Frontal and Cingulate Neural Activity During Conflict and Cognitive Control

Eleonora Bartoli[1], Christopher R. Conner[1], Cihan M. Kadipasaoglu[1], Sudha Yellapantula[2], Matthew J. Rollo[1], Cameron S. Carter[3] and Nitin Tandon[1]

[1]Department of Neurosurgery, University of Texas Health Science Center at Houston, TX 77030, USA, [2]Department of Electrical and Computer Engineering, Rice University, Houston, TX 77005, USA and [3]Center for Neuroscience, University of California, Davis, CA 95616, USA

Address correspondence to Nitin Tandon, Department of Neurosurgery, University of Texas Health Science Center at Houston, 6431 Fannin Street, 77030 Houston, TX, USA. Email: nitin.tandon@uth.tmc.edu

Eleonora Bartoli and Christopher R. Conner contributed equally to the work

Abstract

Cognitive control refers to the ability to produce flexible, goal-oriented behavior in the face of changing task demands and conflicting response tendencies. A classic cognitive control experiment is the Stroop-color naming task, which requires participants to name the color in which a word is written while inhibiting the tendency to read the word. By comparing stimuli with conflicting word-color associations to congruent ones, control processes over response tendencies can be isolated. We assessed the spatial specificity and temporal dynamics in the theta and gamma bands for regions engaged in detecting and resolving conflict in a cohort of 13 patients using a combination of high-resolution surface and depth recordings. We show that cognitive control manifests as a sustained increase in gamma band power, which correlates with response time. Conflict elicits a sustained gamma power increase but a transient theta power increase, specifically localized to the left cingulate sulcus and bilateral dorsolateral prefrontal cortex (DLPFC). Additionally, activity in DLPFC is affected by trial-by-trial modulation of cognitive control (the Gratton effect). Altogether, the sustained local neural activity in dorsolateral and medial regions is what determines the timing of the correct response.

Key words: gamma power, gratton effect, intracranial recordings, stroop task, theta power

Introduction

Cognitive control can be defined as the ability to engage in goal directed behavior and adapt to changing task demands. To accomplish this, it is necessary to continuously adjust the response to changes in external requirements, while inhibiting alternative undesirable responses. A classic cognitive control experiment is the Stroop task, which uses color-words with either congruent or incongruent word-color associations. This task requires participants to inhibit an automatic, overlearned process—reading a word—in order to accomplish the task, for example, name the color in which the word is printed. This simple task has been used to show how the overlearned response is automatically triggered and conflicts with the task-required response if a mismatch is inserted as in the case of incongruent trials.

The brain regions engaged during conflict detection and control have been widely studied (Carter et al. 1995; MacDonald et al. 2000; Van Veen and Carter 2005), and it has been consistently shown that the dorsolateral prefrontal cortex (DLPFC) and medial frontal regions especially the anterior cingulate

cortex (aCC) are involved. These cortical regions are generally conceived to be dynamically interactive, with cognitive control implementation performed by the DLPFC and task-specific monitoring-evaluative processes carried out by the medial frontal cortex and cingulate cortex (CC) (Kerns et al. 2004; Ridderinkhof et al. 2004; Brown and Braver 2005; Sheth et al. 2012). The monitoring-evaluation of the behavioral outcome with respect to external requirements (naming the color while being fast and accurate) drives adjustments in the control on a trial by trial basis (Gratton et al. 1992; Botvinick et al. 2001; Kerns et al. 2004; Ridderinkhof et al. 2004; Shenhav et al. 2013).

Within the aCC, conflict-related activity has been thought to be predominantly located in the region of the cingulate sulcus and associated pre-SMA, rather than on the gyrus per se (Xu et al. 2016). However, given the spatial bias of fMRI to vessels in the sulci, it is unclear if this is due to the biology or due to the measure.

The dynamics and exact spatial localization of the neural correlates of conflict-related behavior can be assessed quite precisely by means of intracranial EEG (icEEG) recordings in humans, which allows us to resolve cortical responses at a millisecond time scale. Prior icEEG studies have demonstrated an association between incongruent color-naming with a response in the gamma frequency range in DLPFC, premotor and supplementary motor areas as early as 500 ms before response (Koga et al. 2011). Further, a theta response that correlates with response times has been localized to the medial prefrontal cortex (Oehrn et al. 2014). A cross-frequency coupling mechanism has been proposed for conflict resolution, wherein gamma responses in the DLPFC are coupled to the phase of theta oscillation in medial prefrontal cortex (Oehrn et al. 2014). However, recent work appears to contradict this finding (Tang et al. 2016), showing a decrease in theta power (combined across lateral, ventral, and medial frontal regions plus CC) during incongruent conflicting trials. Yet, these findings might not be contradictory: they might be related to a fragmented understanding of the different components at play during the detection of conflict and the implementation of cognitive control. Precise spatial co-registration of neural activity across large cohorts of individuals, anatomically exact grouping of recording sites (Conner et al. 2014; Kadipasaoglu et al. 2014; Whaley et al. 2016) and analyses that are specific to brain regions (i.e., not broadly grouped) could help disambiguate local contributions during cognitive tasks.

We performed a Stroop-color-naming experiment in a cohort of 13 patients undergoing intracranial electrode implantation, some with high-resolution penetrating depth electrodes. Our first aim was to characterize the dynamics of gamma power changes during cognitive control in frontal and cingulate regions, while maintaining topological accuracy in anatomical localization across the group. We hypothesized that gamma power would be a clear indicator of the cognitive control process, occurring prominently in the DLPFC and the aCC according to previous literature. More specifically, we predicted that conflict would recruit loci only within the cingulate sulcus and not in the gyrus. Next, we sought to localize regions that manifest conflict-related theta band signal change. Theta has been classically considered a signature of conflict and monitoring, and we would expect a strong increase in theta with conflict trials in the aCC. At the same time, we also sought to identify regions displaying a decrease in theta power during conflict, in order to reconcile previously contradictory findings. Lastly, we performed an anatomically precise grouped analysis based on cortical topology, avoiding grouping electrodes across different anatomo-functional regions, to assess the interaction between conflict and context-dependent effects and to elaborate the mechanisms of trial-by-trial modulation of cognitive control.

Materials and Methods

Sample

A total of 16 participants took part in the experiment. Data from 3 participants were subsequently discarded due to technical issues during the recordings (1 patient) or to excessive interictal epileptic activity in the electrodes of interest (2 patients), yielding a final sample of 13 patients (7 females, mean age = 28.9, standard deviation = 7.9 years). The participants were all patients with medically refractory epilepsy undergoing placement of subdural electrodes (SDE, 6 patients) or stereo-encephalographic electrodes (SEEGs, 7 patients) as part of a presurgical evaluation to localize the site of seizure onset. The interelectrode distance (center to center) was between 3 and 4 mm for the SEEG electrodes. The brain regions sampled with the electrodes were dictated solely by clinical needs and varied across participants (6 left hemisphere, 3 right, 4 bilateral see Table 1). All patients met the inclusion criteria for the study (age > 18 years, IQ > 75, the absence of gross brain structural abnormalities, seizure-free for at least 2 h before and after experimental session) and informed consent was obtained following study approval by our institution's committee for protection of human subjects. Handedness (12 right, 1 left with right hemispheric dominance for language assessed with Wada Test) was assessed using the Edinburgh Inventory (Oldfield 1971).

Task and Stimuli

Stimuli consisted of color-words (e.g., "red") printed in either matching (e.g., in red, congruent trials) or mismatching ink-colors (e.g., in blue, incongruent trials). Five color-words and colors were used to create the stimuli (red, blue, green, brown, and yellow) in order to minimize repetition-priming effects (Ullsperger et al. 2005). Trials were randomized and the frequency of trials belonging to the 2 conditions was balanced (50% congruent, 50% incongruent trials). The number of trials varied across participants (average = 390 trials, range 211–605), depending on the time that each patient had to engage in research activities. Trials associated with incorrect responses (6% of total trials on average), epileptic spikes and recording artifacts (18%) were discarded from subsequent analysis. Additionally, repetitions (same word-color stimulus occurring in consecutive trials, around 9%) were discarded due to the potential confound of repetition effects on conflict adaptation measures (Schmidt 2013). For the analysis focusing on conflict effects, we used all the remaining trials (average = 294 trials, range 147–506). For the analysis taking into account trial by trial adjustments (e.g., Gratton effect) an additional exclusion criterion was applied in which we also excluded trials that were preceded by noisy (i.e., epileptic spike and/or recording artifact) or incorrect trials (average = 241, range = 121–433).

Procedure

Patients were tested at the bedside. The experimental material was presented on a laptop computer placed at eye level, using custom-made presentation script (Python v2.7). A transistor-transistor logic pulse was used to mark stimulus presentation on EEG recordings. EEG signals were recorded from the implanted intracranial electrodes using a BlackRock NeuroPort NSP system

Table 1 Intracranial electrodes implant characteristics

Patient number	Electrode type	Implant side	DLPFC			PreC			SFG	IFG		CC	
			MFG	SFS	IFS	PreCG	PreCS-i	PreCS-s	SFG	IFGop	IFGtr	CG	CS
1	SDE	L	L	L	L	L			L	L	L	L	L
2	SDE	L	L		L	L				L	L		
3	SDE	L	L		L	L				L	L		
4	SDE	L	L		L	L			L	L	L		
5	SDE	L	L		L	L				L	L		
6	SDE	L	L			L				L	L		
7	SEEG	B	B	B	R	R		R	B			R	R
8	SEEG	B	R	B		R	R	R	B			B	B
9	SEEG	B	L	L		L		L	L		L	L	L
10	SEEG	B	L	L	R				R		R	R	R
11	SEEG	R	R		R	R	R	R		R		R	R
12	SEEG	B	B	R	B		R		R		R	R	R
13	SEEG	R	R		R	R	R			R	R	R	R

We summarize for each patient (first column) the type of electrode implant (second column: subdural electrodes, SDE or stereo-encephalographic recording electrodes, SEEG), the hemisphere that was implanted (third column: L, left; R, right; B, bilateral). For each of the 5 ROIs and their the anatomical subdivisions, the actual recorded hemisphere is reported (columns 4–8, L, left; R, right; B, bilateral; an empty cell denotes that no electrodes were recording from that location). The ROIs and anatomical subdivisions (abbreviations only) are reported in the column names.

(Blackrock Microsystems) in 11 patients (2 KHz sampling rate, bandwidth 0.1–750 Hz) or the NeuroFax system (Nihon Koden) in 2 patients (1 KHz sampling rate, bandwidth 0.15–300 Hz). Stimuli were displayed at eye-level on a 15″ LCD screen placed at 60 cm from the patient (500 ms on screen, inter-stimulus interval jittered between 2.5 and 3.5 s). Subjects were instructed to overtly name the ink color in which the word was printed. Vocal responses were recorded through a microphone as an analog input on the same recording system used for EEG recordings (Fig. 1A).

Electrodes Localization

Preimplantation anatomical MRI scans were collected using a 3 T whole-body MR scanner (Philips Medical Systems) and co-registered with a post-implantation CT scan with AFNI software (Cox 1996) to localize SDE electrodes, as previously described (Pieters et al. 2013). SEEG electrodes were manually localized on the CT scan using the center of their artifact. Cortical surface models were reconstructed using FreeSurfer software (v5.1) and imported to SUMA for visualization (Fischl 2012). Spheroids were generated to model each electrode location on the cortical surface model (Pieters et al. 2013).

Anatomical Criterion for Electrode Selection

We defined as regions of interest (ROIs) for the present experiment the following 5 regions: DLPFC defined as comprising middle frontal gyrus (MFG), superior frontal sulcus (SFS), and inferior frontal sulcus (IFS), precentral cortex (PreC, including precentral gyrus (PreCG) and sulcus), the medial aspect of the superior frontal gyrus (SFG), the inferior frontal gyrus (IFG, both opercularis and triangularis) and CC (including the cingulate gyrus and the sulcus). The selection of the ROIs was based on the cortical regions involved in this task (Nee et al. 2007) and further constrained by actual brain coverage in the sample (e.g., parietal cortex was not included as an ROI due to insufficient coverage). For each individual, we identified all electrodes within each ROI in native anatomical space. Cortical gyral and sulcal boundaries were defined using automated parcellation labels from the 2005 Destrieux cortical atlas (Fischl et al. 2004; Destrieux et al. 2010), implemented in FreeSurfer software (Fischl 2012). More specifically, electrodes localized over the following anatomical locations were selected and further analyzed: MFG, IFS, SFS, precentral cortex (PreC, both gyrus and sulcus), SFG, IFG (both opercularis and triangularis part, IFGop and IFGtr, respectively), CC (both gyrus and sulcus, CG and CS, respectively). To enable a topologically accurate population-level analysis, individual subject electrodes were mapped to a standardized cortical surface (MNI N27 template brain, aligned to Talairach coordinate space), using a surface-based normalization strategy as previously described (Saad et al. 2004; Kadipasaoglu et al. 2014, 2016).

Intracranial Recordings

Data were collected and imported into Matlab® and were first evaluated for noise, artifacts, and epileptic activity and to remove line noise (60 Hz). All electrodes with greater than 10 dB of noise in the 60 Hz band or localized to sites of seizure onset were excluded. Trials contaminated by interictal epileptiform spikes were identified (visual inspection of the icEEG traces by the clinician in charge) and the measures related to those trials were discarded from further analysis even if present in a single electrode (including behavioral measures, see Task and Stimuli section). Depending on the recording electrode type, each electrode was re-referenced to a common average of all electrodes (for SDE recordings) or to the average of white-matter placed electrodes (electrodes at least 4 mm away from gray matter boundary in every direction). For each trial, the recording was segmented into 3 second-long windows around the event of interest (Stimulus onset: 0–3000 ms), and a 1 s-long prestimulus baseline window was also extracted (−1200 to −200 ms from stimulus onset). To avoid edge effects due to filtering, 1 s of recording before/after the window of interest was maintained for band power calculations and removed following the analysis. Each trial was band-pass filtered (IIR Elliptical filter, 30 dB sidelobe attenuation) using a filter-bank (100 frequency bands, central frequency increasing logarithmically from 4 to 180 Hz, bandwidth increasing from 1 Hz at lower frequencies to 15 Hz at higher frequencies). A Hilbert transform was used to compute the analytic signal to derive the power in each frequency

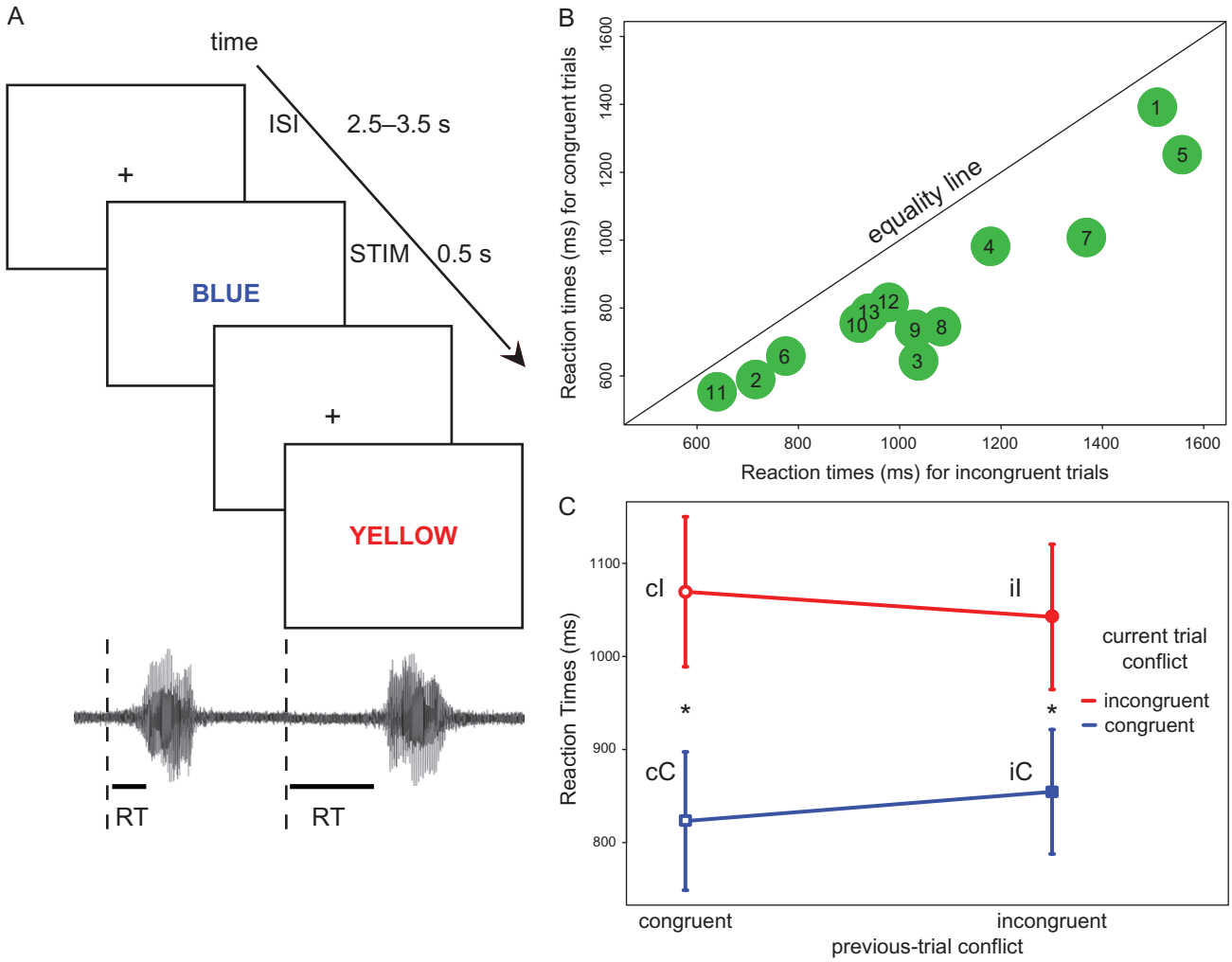

Figure 1. Procedure and behavioral data. (A) Task representation, showing the timing of the events: duration of the interstimulus interval (ISI, jittered between 2.5 and 3.5 s) and of the stimulus (STIM 0.5 s) on the screen. A depiction of the vocal responses, used to extract the RTs is also shown below the task representation. (B) Individual patient behavioral data. Each green dot represents the conflict effect for each patient (1–13) depicted by plotting the mean RT for incongruent trials (x-axis) against the mean RT for congruent trials (y-axis). Dots falling below the diagonal (equality line) indicate longer RTs for incongruent trials (i.e., all patients fall below the equality line, thus all showed longer RTs in relation to conflict). (C) Interaction between previous-trial conflict (x-axis) and current-trial conflict (traces: blue = congruent, red = incongruent trials) on RTs (y-axis). The labels of the different combinations (cC, iC, cI, and iI) are shown close to each mean value (vertical bars represent the standard error of the mean). The asterisks show the post hoc comparisons with a significant difference (with Bonferroni correction): (cI > cC and iI > iC).

band. An electrode specific normalized measure of power was calculated by obtaining the percent change of power with respect to the prestimulus baseline average power, separately for each condition. The time window was then reduced to 2 s after an exploratory analysis on the data, given the return to baseline power in all frequency bands within that window (from stimulus onset to 2000 ms). Subsequently, power in the 50–150 Hz range was averaged to represent gamma power changes. Additionally, power in the 4–8 Hz range was averaged and used to represent theta power percent changes.

Functional Criterion for Electrode Selection

A functional criterion was used to subselect electrodes for further analysis. This additional selection criterion was adopted to refine the inclusion criteria given that (1) some ROIs are difficult to define exclusively by means of anatomical boundaries (e.g., DLPFC) and (2) subselecting electrodes showing some common functional features is a common preprocessing step in many studies dealing with intracranial recordings (Privman et al. 2007, 2011; Flinker et al. 2010; Vidal et al. 2010; Ghuman et al. 2014; Tang et al. 2016). Electrodes displaying a task-related increase in broadband gamma power (50–150 Hz) above a threshold (≥20% increase compared with baseline for at least 150 ms on the average of all trial types—i.e., both congruent and incongruent trials) were identified (Fig. 2A). A total of 83 electrodes were selected, with the following localization: DLPFC had 33 electrodes (15% of the total electrodes in DLPFC in 12 patients—16 in Left MFG, 3 in Right MFG, 4 in L SFS, 3 in L IFS, and 7 in R IFS.); PreC had 30 electrodes (35% of total, surviving in 8 patients—23 in L PreCG, 2 R PreCG, 3 in R PreSi, and 2 R PreSs); L SFG had 3 electrodes (6%—all from the same patient); IFG had 6 electrodes (8%—all in pars opercularis in 3 patients—3 in the left and 3 in the right hemisphere); CC had 11 electrodes (6%—in 5 patients—2 from the right CG and 1 from the right CS and 8 from the left CS). It is possible that some electrodes displaying conflict-related activity were missed due to the specific functional criterion used here and that some electrodes were included just by chance. The

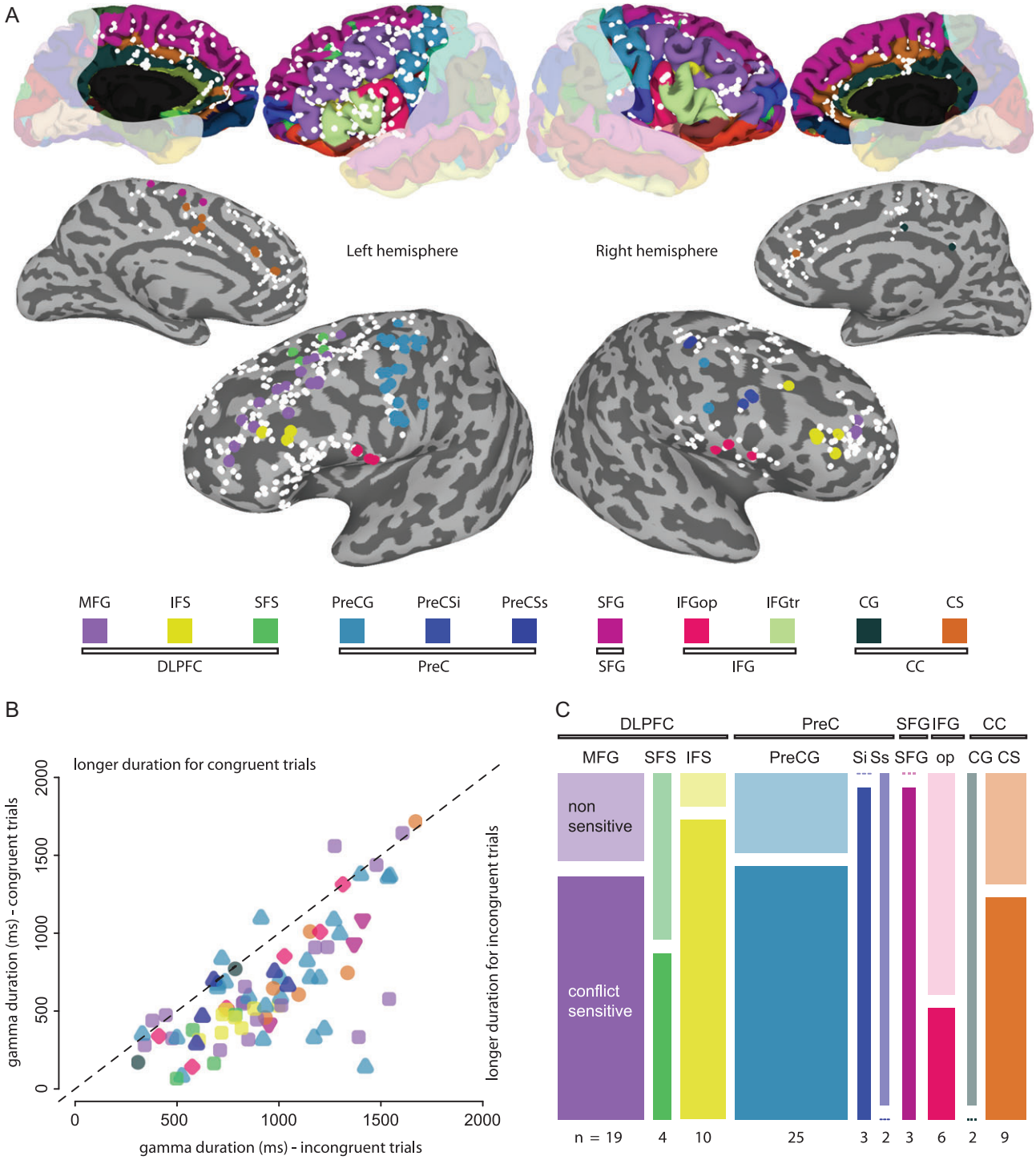

Figure 2. ROI, gamma duration, and conflict-sensitivity. (*A*) On the upper row, all the electrodes in the anatomical locations of interest are depicted on a standardized brain as white spheres and each region is colored according to the Destrieux 2005 parcellation atlas and depicted in the legend. On the second row, the same electrodes are represented on an inflated brain surface that allows for better depiction of electrodes in the sulci. The electrodes surviving the functional activation criterion (≥20% gamma power change for ≥150 ms) are represented by bigger spheres and colored based on anatomical location. (*B*) Duration of significant broadband gamma response during congruent (*y*-axis) and incongruent trials (*x*-axis) represented for each electrode. The marker denoting each electrode is colored according to the electrode location and shaped based on the ROI it belongs to (squares for DLPFC, triangles for PreC, inverted triangles for SFG, diamonds for IFGop and circles for CC). The dashed line represents the equality between congruent and incongruent response duration. The electrodes falling below the equality line show a longer response in the gamma band for incongruent trials. (*C*) For each ROI (DLPFC, PreC, SFG, IFG, and CC) and each anatomical subregion within the ROI (MFG, SFS, IFS, PreCG, PreCSi, PreCSs, IFGop, CG, and CS) the proportion of electrodes contributing to the dataset analyzed is represented by the total area of the rectangles for each region (total electrode count for each region is shown below each rectangle). Each region is subdivided according to the relative proportion of electrodes that are nonsensitive and conflict-sensitive (indicated by graded colors and labeled in MFG). If no electrode contributes to a category, a dashed line is used.

probability of including an electrode by chance was less than 1% (calculated applying the same functional criterion to the inter-trial interval recordings of 671 electrodes and finding 6 electrodes passing the threshold), which is the same rate as reported by a previous work with the similar task (and a different functional criterion) (Tang et al. 2016).

Outline of Analyses Performed

In order to accurately characterize the response-features of the brain regions sampled, and to robustly test hypotheses within the limits of our dataset, different types of analyses were performed. First, we analyzed the behavioral measures at the group-level, to validate classic findings on conflict and trial-by-trial adjustments. Next, we characterized the features of frontal and cingulate regions (response profile, conflict-sensitivity) using gamma power and theta power percent change. This was performed at an individual electrode level for all ROIs, without considering trial-by-trial adjustments. We expected that an increase in gamma power would be detected in the DLPFC and in the aCC, with possible decreases in theta power occurring in fronto-lateral locations as opposed to the CC. We then performed a group-level analysis on gamma power percent change. Three out of 5 ROIs (SFG, IFG, and CC) had small numbers of patients contributing to the data (1, 3, and 5 patients, respectively) and group inferential statistics from these regions were not computed. Therefore, we performed the group-level analysis for the DLPFC (12 participants) and PreC (8 participants) ROIs only. For this analysis, we evaluated both conflict and trial-by-trial adjustments, as for the behavioral analysis. We expected the DLPFC to be sensitive to both conflict and context-effects. For completeness, the analysis was repeated on other frequency bands. The involvement of the CC in conflict is strongly supported by the literature and we performed 2 additional analyses given that we could not analyze the CC at a group level. We performed a connectivity analysis between the DLPFC and the CS electrodes displaying conflict-sensitivity, to evaluate the presence and the direction of intra and inter-regional cross-talk between these 2 ROIs. Lastly, to characterize the brain locations whose activity correlated with response time, we performed a correlation analysis between RT and sustained gamma power activity across all fronto-cingulate electrodes. This analysis was aimed at identifying the regions sensitive to trial-by-trial modulations beyond those analyzable at a group level. Each analysis is described in more detail in the following sections.

Behavioral Measures Analysis

Vocal responses were exported to Audacity® software, down-sampled to 8 KHz and de-noised using spectral noise gating features. The onset of vocal response was determined by automated criterion based on a threshold (exceeding 1.5 standard deviations from the average voltage in the sound recording) and subsequently verified by a human for each trial. The reaction times (RTs) were calculated as the latency between onset of word presentation on the screen and the onset of vocal response and all subsequent analysis was done using R software (Venables and Smith 2008). The RT distribution was tested for violation of normality (Shapiro–Wilk test: $W = 0.93$, $P = 0.006$) and the reciprocal (1/RT) was used as a dependent variable for the analysis ($W = 0.97$, $P = 0.16$). The 1/RTs were analyzed using a within-subject analysis of variance (ANOVA), using as independent factors—conflict (2 levels: congruent or incongruent color-word trials), and previous-trial conflict (2 levels: congruent or incongruent condition on previous trial). The interaction between conflict on the current and previous trial was used to assess trial-by-trial adjustment (the Gratton, or conflict adaptation effect) which are known to affect the RTs. Specifically, incongruent trials preceded by another incongruent trial (iI) are usually faster than incongruent trials preceded by congruent trials (cI). Similarly, congruent trials preceded by congruent trials (cC) are faster than those preceded by incongruent ones (iC). This is due to the increased control on postincongruent trials, which speeds responses to incongruent trials but slows down the facilitation on congruent trials. This is reflected by a modulation of the conflict effect that follows a gradient from slowest to fastest: cI > iI > iC > cC. Whenever an interaction between the "conflict" and "previous-trial conflict" factors reached significance, we performed post hoc comparisons (4 comparisons: iI vs. cI, cC vs. iC, cI vs. cC, and iI vs. iC) using paired t-tests. The significance level corresponding to a true alpha level of 0.01 for four comparisons was 0.0025 following a Bonferroni correction. We did not analyze the neural correlates of behavioral accuracy due to insufficient error trials in our cohort (see "Task and Stimuli" section). We report the untransformed RTs (i.e., not the reciprocal) in the descriptive statistics (means and standard deviations) and in the figures to improve readability.

Individual-Level Analyses: Response Profile

For each electrode surviving the functional criteria, changes in percent power (over the whole spectrum, 4–180 Hz) were obtained for all trials (congruent and incongruent). Time traces of broadband gamma power (50–150 Hz) and theta (4–8 Hz) change from baseline were then extracted. To assess the presence of an increase of the signal with respect to baseline, statistical significance was calculated using a sign-rank test for each time-point, compared with the prestimulus baseline, using an alpha level of 0.01 and applying a false discovery rate (FDR) correction for all samples in the 2000 ms long windows. The onset of response at each electrode was defined as the first time-point that corresponded to a statistically significant difference lasting a minimum of 50 consecutive milliseconds. For all electrodes that showed a significant response (increase from baseline) for both conditions, we assessed if the onset and duration of the response was different between conditions (incongruent and congruent trials) using a paired *t*-test (matched per electrode).

Individual-Level Analyses: Conflict Sensitivity

The difference in response magnitude between congruent and incongruent trials at each time-point was statistically tested by the Wilcoxon Signed-Rank test (alpha of 0.01 FDR corrected) to evaluate the modulation of gamma power depending on condition type. Electrodes with a statistical difference between congruent and incongruent trials were labeled as "conflict sensitive". The percentage of electrodes displaying conflict-sensitivity amongst the electrodes selected by functional criterion was computed for each ROI. We defined as the onset of sensitivity for each electrode as the first time-point displaying conflict-sensitivity. Additionally, the same analysis was repeated using percent signal change in theta power (4–8 Hz) as a dependent variable. The electrodes displaying conflict sensitivity considering the theta band were represented on the brain surface.

Group-Level Analyses: Conflict and Context Dynamics

Given the variable coverage across participants, we performed a grouped analysis only in DLPFC and PreC, where coverage

was relatively more uniform (with 12 and 8 participants contributing to these ROIs, respectively). Gamma power time traces recorded from all electrodes surviving the functional criteria (whether or not they were sensitive to conflict) were used to compute an averaged gamma time trace per condition (iI, iC, cC, cI) across each ROI, within each participant. These time traces were then binned in 8 nonoverlapping 250 ms wide bins and we calculated the average percent gamma power change within each time bin. Data from each ROI was analyzed as a within-subject ANOVA with 3 fixed effects and their interaction terms. The fixed effects modeled were "conflict" (2 levels: congruent/incongruent color-word trials), "previous-trial conflict" (2 levels: congruent/incongruent condition on previous trial), and "timing" (8 levels: from 0 to 2000 ms in 250 ms bins). The *P*-values were computed on corrected degrees of freedom using a Greenhouse–Geisser correction (denoted as p_{ggc} in the result section) whenever a violation of the sphericity assumption was detected (tested using Mauchly test). Whenever an interaction between "conflict" and "previous-trial conflict" factors reached significance (the Gratton effect), post hoc comparisons were performed using paired *t*-tests as described in the behavioral measures analysis section.

Group-Level Analyses: Lower Frequencies

The same analysis described above was repeated for the theta (4–8 Hz), alpha (8–13 Hz) and beta (13–35 Hz) frequency ranges. The results of these additional analyses can be found in the Supplementary Data.

Connectivity Analysis

We performed a connectivity analysis between conflict-sensitive electrodes in the CS and in the DLPFC by means of Granger Causality (GC) implemented using the MVGC Matlab toolbox (Barnett and Seth 2014). Several measures can be used to infer connectivity between brain regions (Blinowska 2011). Here, we adopted GC given our interest in investigating both the strength and the directionality of the connectivity between DLPFC and CC. This restricted the analysis to the data from 2 participants (patient 8: 3 CS, 1 SFS and 2 MFG electrodes; patient 9: 3 CS, 1 SFS and 3 MFG electrodes), thus the sample size limits the generalizability of the present analysis. GC is a statistical measure of causality between time-series data, based on the notion of predictability. The recordings from various electrodes were modeled as a multivariate auto-regressive (AR) process. A 1000 ms window from stimulus onset was used to fit the AR model. GC was calculated on window sizes that ensured stationarity of the data, and allowed for a good fit. Pairwise conditional GC was calculated in the time domain between every pair of conflict-selective electrodes in a patient, ensuring that causality effects due to indirect connections were accounted for. GC was then decomposed in the frequency domain into gamma (70–150 Hz) and theta (4–8 Hz) bands. We compared the GC values between incongruent and congruent color-words associations by mean of permutation testing (5000 permutations) separately for each frequency band and we evaluated statistical significance using an alpha level of 0.05.

Single-Trial Correlation between RTs and Sustained Gamma Power

To further elaborate the role of context-dependent neurophysiological modulation in cognitive control, we assessed whether the correlation of gamma power in each electrode of interest with RTs depending on the previous trial type (trial-by-trial adjustment). We calculated the correlation on all trial types (cC, iC, iI, and cI). The trial-wise gamma power was integrated over time (cumulative sum of gamma power percent change values over each trial epoch), from stimulus onset to response, to obtain a measure of sustained gamma activity at each electrode location for each trial. A Pearson correlation between RT and the sustained gamma power (per trial) was then calculated for each electrode included in the analysis. Only correlations surviving a p-value of 0.01 (FDR corrected) were considered. This correlation identifies all electrodes in which the integrated gamma power over the trial correlates with response time variations. The electrodes displaying a correlation (i.e., relating to the Gratton effect) were represented on the brain surface. The analysis was repeated using a fixed time window (0–1500 ms) to compute the mean gamma power measure. The 2 results were compared.

Results

The results are reported following the order of the analysis as reported in the "Materials and Methods" section.

Conflict Slows Down Response in a Context-Dependent Way

The analysis on the behavioral measures was performed to verify the presence of the classic response time modulations during the task. Overall, incongruent word-color associations led to longer RTs (mean 1056 ± 55 ms) relative to congruent trials (839 ± 49 ms, main effect of "conflict": $F_{1,12} = 53.69$, $P = 9.13 \times 10^{-6}$—from now on *P*-values smaller than 0.001 are reported as $P < 0.001$ and we report exact *P*-values only for values greater than 0.001 to improve readability). RTs on a given trial were not affected by the preceding trial (main effect of "previous-trial conflict": $F_{1,12} = 2.56$, $P = 0.14$), but trial-by-trial modulations affected congruent and incongruent RT differences ("conflict" by "previous-trial conflict" interaction—the Gratton effect, $F_{1,12} = 10.39$, $P = 0.0073$). Post hoc comparisons revealed that incongruent trials had longer RTs with respect to congruent ones when the previous trial was congruent (cI: 1069 ± 81 ms, cC: 823 ± 74 ms, $t(12) = -6.62$, $P < 0.001$, mean of difference 246 ms), as well as incongruent (iI: 1042 ± 78 ms, iC: 855 ± 67, $t(12) = -7.64$, $P < 0.001$, mean of difference 187 ms), with the greatest difference on postcongruent trials (Fig. 1 *B* and *C*). No significant difference could be found either within congruent trials (iC vs. cC, $t(12) = -2.63$, $P = 0.022$) or within incongruent trials (cI vs. iI, $t(12) = -2.14$, $P = 0.053$) when considering the correction for multiple comparisons (alpha level: 0.0025).

Sustained Gamma Band Power Tracks Conflict

The analysis on the response profile of each electrode was aimed at characterizing the modulations occurring in the gamma power band according to the presence of conflict, testing both onset and duration. A statistically significant response to both congruent and incongruent trials with respect to baseline was found for 92% of the electrodes selected by functional criteria (76 out of 83 electrodes). The remaining 8% electrodes (7 electrodes—3 in the CS, 2 in IFS, 1 in MFG and 1 in PreCG) responded only during incongruent trials.

For all the electrodes exhibiting a significant response in both conditions, we tested whether a difference was present in the onset and in the duration of the gamma power change, depending on the condition. The onset time was not different

between congruent and incongruent trials ($t(75) = 0.851$, $P = 0.397$). However, the response duration was about 300 ms longer for incongruent trials (Fig. 2B, response to incongruent trials 292 ± 31 ms longer than to congruent trials, $t(75) = 9.408$, $P < 0.001$), indicating a sustained response in the gamma power band associated with conflict.

Gamma Band Power Increases following Conflict Across Fronto-Cingulate Regions

The analysis of conflict-sensitivity was performed to individuate all brain locations exhibiting an increased activity during conflict and the features of this conflict-sensitivity. In the electrodes showing task-related activity, 70% were conflict-sensitive (58 of 83 showing a difference between congruent and incongruent trials). For all conflict-sensitive electrodes, higher gamma power was seen in incongruent versus congruent trials. In general, the electrodes not showing a sensitivity to conflict were evenly distributed across the ROIs, which thus showed a mixture of conflict-sensitive and nonsensitive electrodes (Fig. 2,C). All the analysis and results reported here are related to data aligned to stimulus onset. Indeed, some aspects of conflict monitoring are more precisely measured in stimulus-aligned data and intrinsically linked to the modulation of RTs (Carter and van Veen 2007; Yeung et al. 2011). For completeness, the data was re-analyzed by realigning the traces to response times (−1500 to 500 around RT). The pattern of response was similar to what was found in the stimulus-locked analysis (Fig. 3 A–B) and the majority (44/58) of electrodes was sensitive to conflict in both time windows (0–2000 ms from stimulus onset and −1500 to 500 ms around response time; See Supplementary Data, Response locked analysis).

Detailed below are the conflict-sensitivity results for each ROI. The average onset time and duration of the dissociation between congruent and incongruent trials is reported.

Dorsolateral Prefrontal cortex: The majority of electrodes in both the left and right hemisphere (74%, 14 out of 19) in MFG dissociated based on conflict. On average, the dissociation began at 593 ± 41 ms after stimulus onset and lasted 466 ± 81 ms (Fig. 3 A–C). Within the IFS the vast majority of electrodes (90%, 9 out of 10), in both hemispheres showed a conflict effect. This conflict-related dissociation started on average 517 ± 39 and lasted 424 ± 95 ms. In SFS, half of the electrodes were dissociating (50%, 2 out of 4). Conflict-sensitivity began at 677 ± 11 ms and lasted 194 ± 150 ms.

Precentral cortex: The majority of the electrodes recording from the PreCG in either hemisphere showed conflict-sensitivity (76% dissociating, 19 out of 25). The onset of dissociation was on average 795 ± 60 ms, lasting 366 ± 54 ms. No electrodes in the superior part of the precentral sulcus (PreCSs) showed conflict-sensitivity, while all 3 of the electrodes in the inferior part (PreCSi) did. The onset of the dissociation started at 654 ± 89 ms and lasted 134 ± 10 ms.

Medial SFG: In SFG, all electrodes were conflict-sensitive (3 of 3, in both time windows), all were located in the left hemisphere. Gamma power dissociated between conditions at 750 ± 93 ms for 640 ± 137 ms duration.

Inferior frontal gyrus: In IFG pars opercularis 2 electrodes out of 6 were conflict-sensitive (1 in a language dominant right hemisphere and 1 in the left hemisphere, from a different patient). Conflict selectivity started 570 ± 112 ms, lasting 384 ± 169 ms. The 4 remaining electrodes were nonsensitive.

Cingulate cortex: No conflict-sensitive electrodes were found in the gyrus, (2 nonsensitive out of 2 electrodes) but electrodes in the sulcus showed clear conflict sensitivity (CS: 67%, 6 out of 9). All of these were located in the left hemisphere and the dissociation started at 644 ± 104, lasting for 343 ± 132 ms.

Theta Power Highlights Separate Regions Involved in Conflict and No Conflict Trials

We additionally performed individual-level analyses (response profile and conflict sensitivity) focusing on theta (4–8 Hz) power percent change (Fig. 3D–E). This analysis aimed at addressing the recent contradictory finding on the direction of theta-band power modulation during conflict (Tang et al. 2016). Theta power was increased for incongruent trials with respect to congruent trials in dorsal-frontal locations and in the CC, whereas there was an increase for congruent trials in more fronto-lateral and ventral locations (Fig. 3F). For sake of brevity, we report in detail the conflict-sensitivity results for the CC only.

Cingulate cortex: In the gyrus (CG), 1 out of the 2 electrodes showed a significant increase in theta power with respect to baseline during both congruent and incongruent trials, which was not significantly different between conditions (no conflict-sensitive electrodes in CG). Of the 9 electrodes in the cingulate sulcus, 5 showed a significant theta increase for both congruent and incongruent trials, 2 showed a theta response only during incongruent trials and 2 never showed a significant change in theta power. Regarding conflict-sensitivity, 5 electrodes were conflict-sensitive, and 4 were not. All electrodes showing a theta-sensitivity to conflict also showed a gamma-sensitivity. Additionally, conflict-sensitivity response started around the same time in both frequency bands (theta: 725 ± 88 ms from stimulus onset; gamma: 739 ± 15 ms—recalculated on the 5 electrodes with conflict-sensitive in both frequency bands for comparability) but lasted longer in the gamma (495 ± 143 ms) than in theta band (182 ± 48 ms) (Fig. 3D–E).

Gamma Power in the DLPFC—But Not in Motor Cortex—is Sensitive to the Gratton Effect

The group-level analysis allowed us to test the full experimental design, assessing both conflict and the interactions between conflict and the context in which this occurs and closely paralleling the analysis performed on the behavioral measures.

DLPFC: Gamma power percent change was on average higher for incongruent trials (34.35 ± 2.78%) compared with congruent ones (22.07 ± 1.95%) (main effect of "conflict": $F_{1,11} = 27.45$, $P < 0.001$). The magnitude of the power change varied significantly within the time window analyzed ("timing" main effect: $F_{7,77} = 12.59$, $p_{ggc} = 0.004$, P-value corrected for departure from sphericity using Greenhouse–Geisser correction, denoted with p_{ggc}), starting from low values (11.08 ± 1.6% in the 0–250 time bin) reaching highest values around 500–750 ms after stimulus onset (64.41 ± 6.59%) and returning to baseline around 1.5–2 s after stimulus presentation (10.69 ± 1.88% in the 1750–2000 ms time bin). The dynamics of the conflict effect (i.e., the variation over time of the difference between congruent and incongruent trials) were captured by the interaction between the conflict factor and the timing factor (Interaction "conflict by timing": $F_{7,77} = 7.3236$, $p_{ggc} = 0.002$). Congruent and incongruent trials were not different from each other immediately after stimulus onset, but begin to diverge around 500 ms, reaching a maximum between 500 and 1000 ms (30% difference). Post hoc testing for each time epoch (8 comparisons, the alpha level equivalent to a 0.05 is 0.05/8 = 0.00625) showed that the incongruent trials had higher power change values starting at

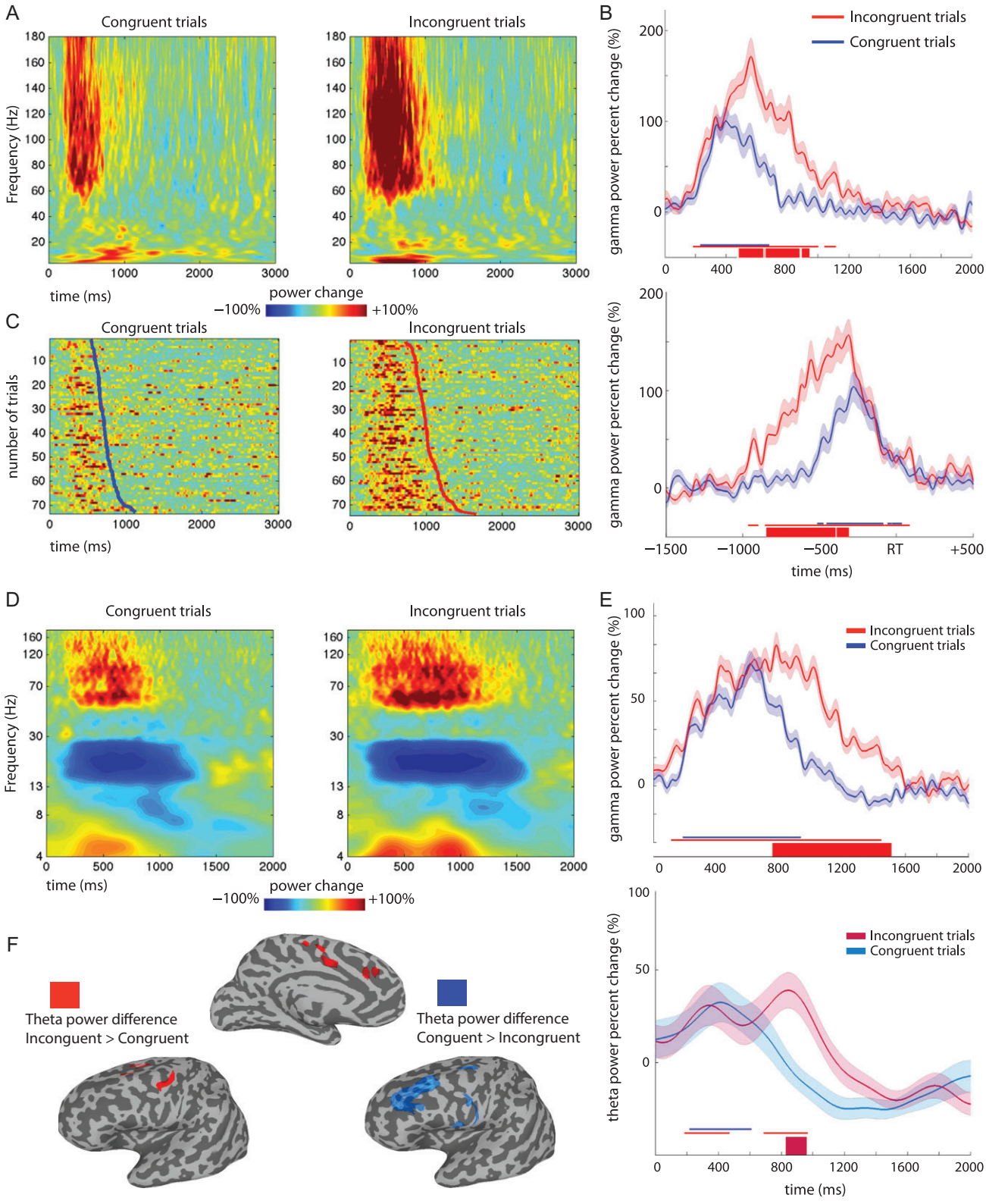

Figure 3. Response profiles and conflict-sensitivity. (*A–C*) Example of 1 typical MFG electrode. (*A*) Averaged time-frequency plot of the whole spectrum for congruent and incongruent trials. Data are shown from stimulus onset (at 0 ms on the *x*-axis) to 3 s after stimulus onset. (*B*) Time traces of gamma power (50–150 Hz) change for incongruent (red) and congruent (blue), locked to stimulus onset (upper) and response time (lower). Shading around the traces represents one standard error of the mean at each time-point. The thin colored lines above the *x*-axis show the time points at which the gamma power was statistically different from baseline and are used to report the onset and duration of response. The thick line represents time points with a significant difference in gamma power between congruent and incongruent trials (used to define conflict sensitivity, and its timing). (*C*) Raster plots of single-trial gamma power sorted by RT (solid line) showing congruent and incongruent trials. (*D*) Time-frequency maps of power change shown for 1 electrode recording from the cingulate sulcus (patient 8) during congruent and incongruent trials.

500–750 ms and lasting until 750–1000 ms (*P*-values for each time window: 0–250: $P = 0.68$, 250–500: $P = 0.011$, 500–750: $P = 0.00013$, 750–1000: $P < 0.0001$, 1000–1250: $P < 0.0001$, 1250–1500: $P = 0.0005$, 1500–1750: $P = 0.037$, 1750–2000: $P = 0.23$).

A trial by trial modulation, classically defined as the Gratton effect (Interaction *conflict* by "previous-trial conflict": $F_{1,11} = 8.75$, $P = 0.013$) was also detected. The difference in gamma power between incongruent and congruent trials was larger when these were preceded by congruent trials (cI 35.39 vs. cC: 20.11%) than preceded by incongruent trials (iI: 33.29 vs. iC: 24.03%). Post hoc comparisons indicated that congruent trials were different from each other depending on the previous trial type (cC: 20.11%, iC: 24.03%, $t(95) = 3.74$, $P = 0.0003$ uncorrected, significant considering the Bonferroni corrected alpha = 0.0025), whereas incongruent trials were not (cI: 35.39%, iI: 33.29%, $t(95) = -2.29$, $P = 0.024$ uncorrected, not significant with correction). Comparisons between congruent and incongruent trials were significant when preceded by congruent trials ($t(95) = -7.08$, $P < 0.001$) as well as incongruent trials ($t(95) = 5.39$, $P < 0.001$). Thus, the Gratton effect was driven by the modulation of gamma power change within congruent trials, which was significantly higher on postincongruent trials. The magnitude of the Gratton effect varied over time, as shown by a significant 3-way interaction between "conflict" and "previous-trial conflict" and "timing" factors ($F_{7,77} = 3.3349$, $p_{ggc} = 0.024$). No other main effects or interactions reached significance levels (e.g., no main effect of "previous-trial conflict" was present; Fig. 4A). These data are consistent with gamma power in DLPFC being sensitive to conflict detection as well as to trial-by-trial reactive cognitive control. The modulation of the power resembles the modulations observed in the response times, linking the activity in this ROI with the behavioral performance.

PreC: Gamma power increase during incongruent trials was also notable in precentral regions (average percent change for incongruent trials: 31.91 ± 2.29%; for congruent trials: 23.45 ± 1.82%, main "conflict" effect $F_{1,7} = 14.61$, $P = 0.006$). The overall time course of evolution of gamma power was similar to that in DLPFC ("timing" main effect $F_{7,49} = 5.09$, $p_{ggc} = 0.026$), with low values at stimulus onset (14.99 ± 2.2% in the 0–250 time bin), peaking after 500–750 milliseconds (50.8 ± 4.69%) and returning to baseline values around 2 s from the stimulus presentation. The temporal evolution of the conflict effect was also similar to that in the DLPFC, although showing a less dramatic but more sustained difference ("conflict" by "timing" interaction: $F_{7,49} = 4.81$, $p_{ggc} = 0.021$). Post hoc testing for each time epoch (8 comparisons, alpha level = 0.00625) showed that the incongruent trials had higher power change values starting at 500–750 ms and lasting until 1750–2000 ms (*P*-values for each time window: 0–250: $P = 0.29$, 250–500: $P = 0.33$, 500–750: $P = 0.0006$, 750–1000: $P < 0.0001$, 1000–1250: $P = 0.002$, 1250–1500: $P = 0.004$, 1500–1750: $P = 0.0017$, 1750–2000: $P = 0.0018$). No other main effects or interactions reached significance, showing that the "previous-trial conflict" by "conflict" interaction did not modulate power in precentral areas (Fig. 4B), as opposed to the DLPFC results.

Beta Band is Sensitive to Higher Control Requirements

Power percent change in the beta band (13–35 Hz) in DLPFC was modulated by the conflict in the previous trial: it was decreased on postincongruent trials with respect to postcongruent ones (3.01 ± 1.49% vs. 8.41 ± 1.81%, main effect of "previous-trial conflict" $F_{1,11} = 4.91$, $P = 0.048$). A similar result was found considering PreC. Beta was the only frequency band to show a modulation according to the previous-trial conflict. Power in the beta band (and in other frequency components) was not modulated by the interaction between "conflict" and "previous-trial conflict", as opposed to gamma in DLPFC. Both alpha and theta in the DLPFC showed sensitivity to conflict. The complete results can be found in the Supplementary Data.

Increased Connectivity within the Cingulate and from the Cingulate to the DLPFC

The connectivity analysis between CS and DLPFC was done only in patients who had conflict sensitive electrodes in these 2 areas—this restricted the analysis to the data from 2 participants (patient 8: 3 CS, 1 SFS and 2 MFG electrodes; patient 9: 3 CS, 1 SFS and 3 MFG electrodes). Given that the small sample being considered, it is important to stress that these results should be viewed more as a proof of concept rather than as a conclusion that can be extended to the population. When considering the gamma band, there was an increase in the connectivity for incongruent trials with respect to congruent ones from the CC to the DLPFC (1 CS electrode to 1 MFG electrode in patient 8, $P < 0.05$). Additionally, the connectivity within the CC was also increased (1 CS electrode to another CS electrode in both patients 8 and 9, $P < 0.05$). The intracingulate increased connectivity pattern was mirrored in the theta band (for patient 8, same CS to CS electrodes; no significant changes in connectivity where present considering patient 9).

Sustained Gamma Power Tracks Context-dependent Behavioral Modulations

The main goal of the correlation analysis was to disentangle the neural substrates underpinning the trial-by-trial modulation effect. In particular, in DLPFC the gamma power percent change during congruent trials was modulated by the preceding trial, as reported in the previous result section. We therefore calculated correlation coefficients for cumulative gamma power—a surrogate for total local neural processing over the epoch—for all 4 subsets of trials. Around one-third of the electrodes showed a correlation for iC: ($n = 27$, 35% of total analyzed electrodes). A similar proportion of electrodes showed a significant correlation for cC ($n = 23$ electrodes, 28% of total analyzed electrodes), iI ($n = 23$), and cI ($n = 25$) trials. For postincongruent congruent trials (iC), the correlation ranged between 0.29 (in PreCG) to 0.76 (in MFG). Considering postcongruent congruent trials (cC), the correlation values ranged from −0.34 (only 1 electrode had a significant negative correlation with RT while only considering cC

Frequency (*y*-axis) is represented using a log-scale to elaborate contributions of lower frequencies. (*E*) Time traces of gamma (upper) and theta (lower) power change at the same CS electrode (patient 8). Shadings around traces represent one standard error of the mean at each time-point. The thin colored lines above the *x*-axis show the time points at which the gamma power was statistically different from baseline and are used to report the onset and duration of response. The thick line represents time points with a significant difference in gamma power between congruent and incongruent trials (used to define conflict sensitivity, and its timing) Note that the onset of conflict sensitivity is similar across the 2 frequency bands, while lasting longer for gamma. (*F*) Surface-based representation of electrode locations showing a difference in theta power between congruent and incongruent trials. In red are shown the locations where theta power is higher for incongruent trials, in blue for congruent trials.

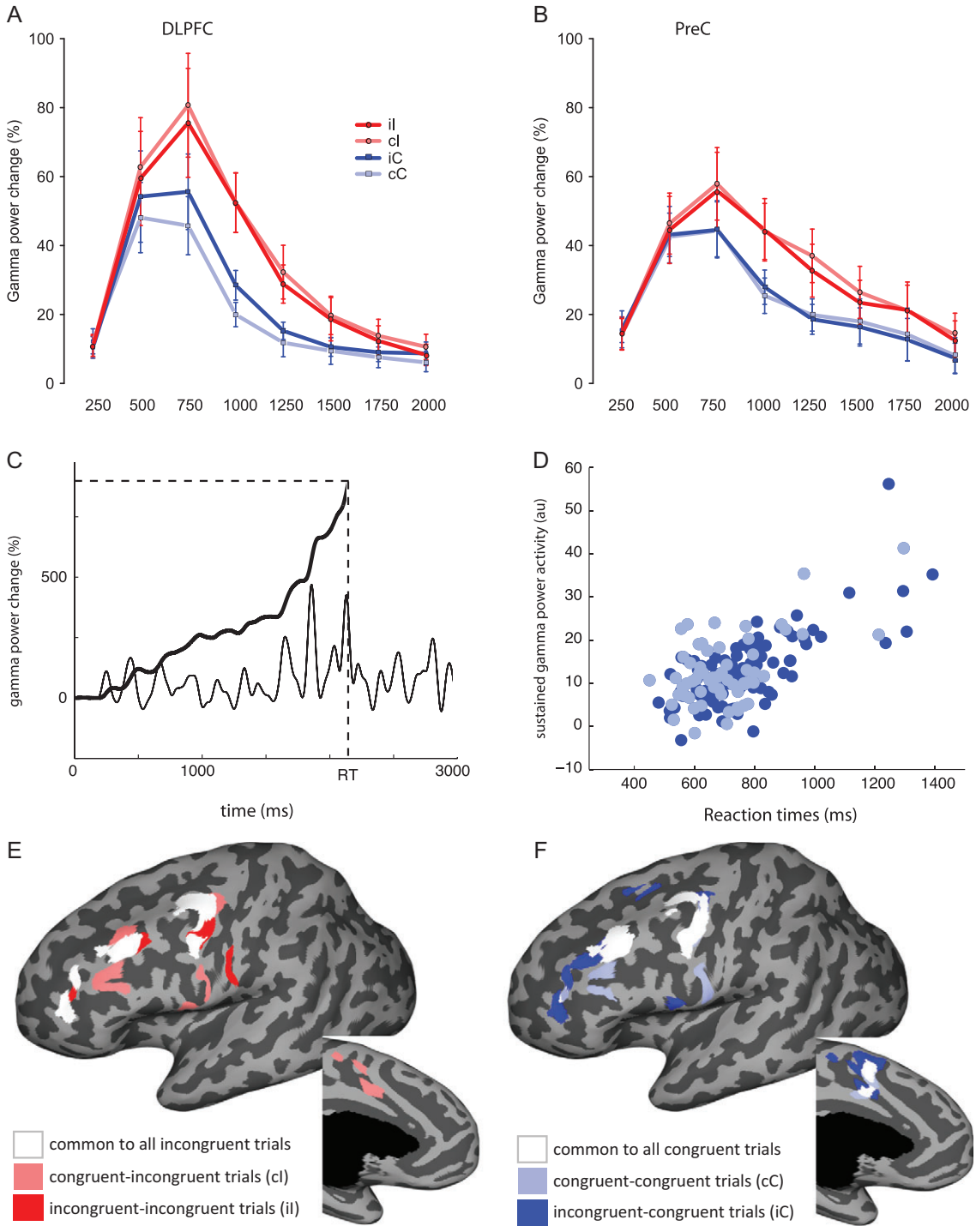

Figure 4. Conflict and trial-by-trial modulations. (*A*) DLPFC. (*B*) PreC. In both panels, the y-axis represents gamma power percent change. The x-axis represents averaged values in 250 ms wide time bins (e.g., 250 refers to an average of values between 0 and 250 ms, and so on). Red and blue traces (with circles and squares as markers) represent incongruent and congruent conditions respectively. Light-color traces represent the postcongruent trials (cI in light red and cC in light blue), saturated-color traces the postincongruent trials (iI in red and iC in blue). Bars represent standard error of the mean. (*C*) example of single-trial gamma power change (black thin line) integrated over time (black thick line) from stimulus onset (0 ms) to the RT (dashed vertical line) to obtained the cumulative gamma power value (horizontal dashed line) that is used as an index of sustained gamma activity. (*D*) Example of the correlation between gamma power cumulative values and RTs calculated on one electrode using congruent trials (cC and iC, in light blue and dark blue) separately. (*E*, *F*) Surface-based representation of the regions exhibiting a significant correlation (for the left hemisphere only, both lateral and medial views) between gamma power and RTs considering incongruent trials (*E*: cI in light red; iI in dark red; common to both in white) and for congruent trials (*F*: cC in light blue; iC in dark blue; common to both in white).

trials: this electrode was located in left PreCG) to 0.65 (MFG electrode) with a median value of 0.49. Postincongruent incongruent trials (iI) had values ranging between 0.28 and 0.61 (min and max both in PreCG) and cI between 0.30 (IFGop) and 0.65 (PreCG). A higher number of electrodes showed a correlation between gamma power and RTs when considering the

cumulative power during the whole trial duration (from onset to RT as opposed to the mean power over a fixed-duration window, see Supplementary Data, Correlation analysis section), proving that a measure mixing the magnitude and the duration of the sustained activity yields stronger results than a measure based on the activity over a fixed time window alone.

The spatial distribution of the regions displaying significant correlations (Fig. 4*C–F*) revealed overlapping sets of regions that correlated with all the different trial types. Gamma power in left posterior MFG, dorsal PreCG, right IFGop, right anterior MFG, and IFS correlated with RTs for all trial types (see Supplementary Data Fig. S2). Some loci were unique to postincongruent trials (iI and iC): dorsal DLPFC (SFS) and left medial frontal cortex (SFG) were specific to iC trials, bilateral ventral precentral cortex loci were specific to iI trials. More ventrally distributed sites showed significant correlation values for postcongruent trials (left IFS, right PreCSi, ventral portions of the left PreCG) with a differential involvement of medial regions (left dorsal CS for cC trials, left dorsal and right anterior CS for cI and iC trials). Intriguingly, no cingulate locations correlated with RTs on iI trials.

Discussion

Our work assesses the neural dynamics of cognitive control, using intracranial recordings in participants performing the classic Stroop-color-naming task. Our behavioral data are in agreement with previous findings, showing longer RTs during incongruent trials (i.e., where a conflict between word and color is present, increasing cognitive control demands) versus congruent ones (same word-color association). Also, the difference between incongruent and congruent trials reflected the trial-by-trial adjustments in performance associated with conflict monitoring, showing that conflict-related effects are smaller when considering trials preceded by incongruent trials—the Gratton effect.

A Sparse Coding Structure in Prefrontal Cortex Underlies Conflict Processing

Our characterization of response profiles for each electrode, based on the onset and duration of gamma power during congruent and incongruent trials, revealed that electrodes mainly located in the cingulate sulcus showed a response specific only to incongruent trials. No electrodes (in any ROI) showed a response to congruent trials alone. Crucially, the duration of gamma power increase was longer for incongruent trials, suggesting that sustained local neural activity (Cardin et al. 2009) underlies the implementation of cognitive control, consistent with computational modeling studies of conflict monitoring (Botvinick et al. 2001; Yeung et al. 2004). Our classification of electrodes as conflict sensitive or nonsensitive based on gamma power change during congruent versus incongruent trials revealed that locations sensitive to conflict are distributed across frontal and CC, intermixed with locations whose activity is not modulated by higher-load situations (Fig. 2). This distributed pattern indicates that a sparse coding structure underlies the representation of task rules, conflict and cognitive control, with sustained activity being driven by the presence of conflict, until this conflict is resolved (Fig. 3).

Theta Power is Specifically Localized to the Cingulate Sulcus

Our analysis reveals that conflict processing is associated with higher power in the theta band within CC, supporting a key role for theta during conflict detection. This is in agreement with previous studies (Cavanagh and Frank 2014; Oehrn et al. 2014; Reinhart et al. 2015) and challenges a recent report showing a decrease of theta power related to conflict (Tang et al. 2016). Given the specific topology of theta activity, we suggest that those results might have been confounded by pooling across multiple anatomical locations. Indeed, by analyzing theta power at a single electrode level we were able to find an increase in theta power during congruent trials at specific sites in anterior and fronto-lateral regions. These locations were segregated from the medial and dorsal ones that displayed an increase during conflict (Fig. 3).

Intriguingly, there was an almost perfect match between the electrodes displaying conflict-sensitivity in theta and in gamma frequency bands within the cingulate sulcus—electrodes classified as conflict-sensitive based on gamma power difference also displayed a theta power difference. The onset of the conflict-sensitivity in gamma and theta was similar, but gamma power changes were more sustained, suggesting distinct functional roles for these 2 frequency bands: local processing (indexed by gamma activity), could be integrated across neural ensembles by long-range interactions (indicated by the theta band activity). Indeed, the coupling between theta and gamma power has been implied as mechanism for the coordination and integration of activity across distributed cortical networks (Canolty et al. 2006; Voytek and Knight 2015). Here, we show that cognitive control relies on local gamma power sustained activity spread in fronto-cingulate location. Theta power modulations were more complex, showing different loci encoding for conflict and no conflict situations. Future studies are needed to clarify how adjacent cortical loci modulate theta power in a variable way and whether this is critical to the engagement of distinct circuits based on the presence or absence of conflict.

Context-Dependent Modulation of Gamma Power in Prefrontal Areas

Gamma power changes in both DLPFC and PreC regions were modulated by conflict, with a peak in gamma power between 500 and 750 ms and a maximal difference between congruent and incongruent trials between 750 and 1000 ms, sustained until 1500 ms. A context-dependent modulation, trial-by-trial adjustments influencing the magnitude of the conflict response, was detected in DLPFC but not in the PreC. This modulation mirrors the well-studied behavioral effect, characterized by an increase of RTs on trials with no conflict when preceded by a conflict trial. The interaction was driven by an increase in power in congruent trials that were preceded by incongruent trials (iC) versus congruent trials preceded by another congruent trial (cC). A similar trend was present for incongruent trials (iI vs. cI). This reveals that increased cognitive control requirements lead to gamma power modulation in both DLPFC and precentral cortex, whereas DLPFC alone is affected by the context in which control needs to be exerted (Fig. 4). This result clearly elucidates that motor regions are affected by the presence of conflict, but the implementation of control over the response tendency affects regions upstream in the network, in DLPFC and not at the motor output level. However, the observed pattern of DLPFC modulations is not fully concordant with classical theoretical hypotheses on cognitive control implementation. On the one hand, DLPFC gamma was greater for congruent trials preceded by high conflict (iC) versus low conflict (cC), an important prediction of classical conflict-control loop theory. On the other hand, this was not the case for incongruent trials, where there was a nonsignificant trend for gamma to be lower for iI than cI trials. Furthermore, in

the present study higher activity occurs along with longer RTs, while the expected result for cognitive control would be higher activity with an increase in RT on iC trials but a decrease in RTs on iI trials. Therefore, DLPFC gamma shows a complex pattern of activity: some features (congruent effect on gamma power, positive correlation with RTs) are suggesting it reflects the level of conflict (Egner and Hirsch 2005; van Steenbergen and Band 2013), while other features (interaction with previous trial history, higher activity for congruent trials preceded by conflict) are consistent with a relationship with control implementation. Hence the evidence from the present data suggests that DLPFC gamma power likely reflects both conflict and its regulation. One possible reason for the failure to show higher gamma activity on iI trials (vs. cI) could be that if gamma reflects the combined activity between conflict processing and cognitive control, the reduction in activity associated with reduced conflict on iI trials may offset any increase in gamma associated with control implementation. One of the key predictions of conflict-control theory (Botvinick et al. 2004; Carter and van Veen 2007) is a dissociation between the aCC and the DLPFC, with the former detecting conflict and the latter implementing control. The present study suggests a more nuanced dissociation, with a distinct role for theta in the aCC responding to conflict, evidence for conflict-related gamma in DLPFC, along with some evidence for a role for DLPFC gamma in reactive cognitive control (the Gratton effect).

MFG locations can show both correlates of reduced conflict (as in the present work) and of increased control (Egner and Hirsch 2005). Can we reconcile these observations with the classic roles assigned to prefrontal cortex in control? A possibility is that different functions might arise from the entrainment of different rhythms (or by their de-synchronization), yet within the same regions. This would also possibly reconcile the finding that dorsal aCC firing rates increase following conflict (Sheth et al. 2012), contradicting classical fMRI results (Kerns et al. 2004) and the role of the cingulate in conflict detection. Following this speculation, it is tempting to suggest that some patterns of communication among neural ensembles might relate to conflict processing (e.g., detectable by examining gamma power and BOLD signal), while others might be carrying information regarding control requirements (firing rates and beta band power modulation).

Sustained Gamma Activity Tracks Response Time: Conflict Processing Versus Conflict Resolution

Finally, we tested whether the neural assemblies responsible for adjustments of cognitive control were broader than the DLPFC. Indeed, existing studies strongly point out at a key role of medial prefrontal regions in such context-dependent effects (Kerns et al. 2004; Sheth et al. 2012), which we could not analyze at a group level as done with the DLPFC. Most of the electrodes showing a response to conflict were located along the length of the cingulate sulcus. As a note, we report that in 2 CS electrodes (patient 8), gamma power was significantly higher on postincongruent trials (iC vs. cC trials, Wilcoxon Signed-Rank test $P < 0.05$ corrected for multiple comparisons), analogous to the result observed in DLPFC, thus mirroring the reduced conflict effect. These 2 CS electrodes were the same exhibiting an increase in connectivity for conflict within the cingulate and from the cingulate to the DLPFC. Therefore, these loci within the cingulate sulcus increased their influence on other regions during the detection of conflict, while themselves being sensitive to the context-dependent modulation effects.

To map all the regions exhibiting context-dependent modulations, we correlated the response time on each trial with the sustained gamma band power recorded from each fronto-cingulate electrode. This analysis allowed us to have a map of the regions that were displaying more sustained activity in relation to prolonged response times to the task. Left posterior MFG, dorsal PreCG, right IFGop, right anterior MFG, and IFS correlated with the response time regardless of the conflict and control loads (Fig. 4). Other loci were correlated only with specific trial types, as the dorsal SFS and medial SFG for iC trials and bilateral ventral precentral areas for iI. This correlation carries important implications for the understanding of the neurobiology of cognitive processes—more prolonged and greater activity across a distributed network, rather than a greater amplitude of activity over a fixed-duration, correlates robustly with the response time. This observation fits with the existing models of conflict (Botvinick et al. 2004). These models account for behavioral effects by means of the simultaneous activation of competing representations, where a conflict monitoring unit gets activated to bias the network toward task demands. This predicts more sustained activity during incongruent trials and a direct influence over control. From a neural perspective, this would be translated by a different cross-talk between lateral and medial regions depending on the context in which conflict occurs. Postincongruent trials are characterized by increased control that should predict faster RTs on incongruent trials. Here we show partially overlapping distributed fronto-cingulate locations sensitive to trial-by-trial modulations of conflict, which track the reduced conflict rather than the increased control.

The increased influence of cingulate regions on dorsolateral prefrontal regions is the putative mechanism that mediates context-dependent effects. Our connectivity data is far too limited to test this hypothesis in the present work. It has been shown that the Gratton effect is abolished after cingulate ablation (Sheth et al. 2012), pointing out at a possible key role of this region in the regulation of cognitive control. However, trial-by-trial modulations have been shown to be sensitive to different parameters, such as practice, raising some questions about the specificity of that effect (van Steenbergen et al. 2015). Additionally, conflict adaptation effects can occur within a trial (Scherbaum et al. 2011), complicating further the possibility of dissociating contributions from control and conflict processing via trial-by-trial adjustments. Altogether, these arguments along with our results highlight the need for a deeper understanding of cognitive control implementation mechanisms, which might stem from interactions far more complex than previously suggested.

Conclusions

Our findings provide clear evidence to support the roles of specific fronto-cingulate regions during dynamic cognitive control. These regions contain neuronal ensembles sensitive to cognitive control requirements, that are intermingled with more broadly task responsive locations, suggesting a sparse coding behind the representation of task rules for cognitive control and conflict detection. Gamma band activity in fronto-cingulate regions is sustained during conflict between task rules and response tendencies. In the cingulate sulcus, frequency-specific power modulations track conflict and possibly the coordination of neural ensembles involved in cognitive control implementation, with transient theta increases coupled to sustained gamma power responses. This is in agreement with fMRI and lesion studies on the role of this region in cognitive control and clarifies previously contradictory findings on the role of theta and of

the CC during conflict. In dorsolateral prefrontal regions gamma power increases are modulated by context effects, which affect the ability to efficiently implement cognitive control on a trial-by-trial basis. Indeed, trial-by-trial modulations of cognitive control reveal the recruitment of several fronto-lateral and cingulate locations that correlated with response time, tracking conflict processing. Altogether, this work yields valuable insight about the precise cortical topography of the neurophysiological basis of cognitive control. Future studies are needed to clarify the neural underpinning of conflict resolution, which might not be detectable as an increase in local activity in a specific region, but rather be manifest as differential entrainment of brain rhythms in a distributed prefrontal-cingulate network.

Supplementary Material

Supplementary data are available at *Cerebral Cortex* online.

Notes

This work was supported by NIH (grant R01DC014589). We are deeply indebted to the patients who willingly participated in this study, the epilepsy neurologists (Drs. Slater, Kalamangalam, Hope, and Thomas) who provided care to these patients, and the nurses and technicians in the Epilepsy Monitoring Unit at Memorial Hermann Hospital who helped make this research possible. The authors declare no competing financial interest. *Conflict of Interest*: None declared.

References

Barnett L, Seth AK. 2014. The MVGC multivariate granger causality toolbox: a new approach to Granger-causal inference. J Neurosci Methods. 223:50–68.

Blinowska KJ. 2011. Review of the methods of determination of directed connectivity from multichannel data. Med Biol Eng Comput. 49:521–529.

Botvinick MM, Braver TS, Barch DM, Carter CS, Cohen JD. 2001. Conflict monitoring and cognitive control. Psychol Rev. 108: 624–652.

Botvinick MM, Cohen JD, Carter CS. 2004. Conflict monitoring and anterior cingulate cortex: an update. Trends Cogn Sci. 8: 539–546.

Brown JW, Braver TS. 2005. Learned predictions of error likelihood in the anterior cingulate cortex. Science. 307: 1118–1121.

Canolty RT, Edwards E, Dalal SS, Soltani M, Nagarajan SS, Berger MS, Barbaro NM, Knight RT. 2006. High gamma power is phase-locked to theta oscillations in human neocortex. Science. 313:1626–1628.

Cardin J a, Carlén M, Meletis K, Knoblich U, Zhang F, Deisseroth K, Tsai L-H, Moore CI. 2009. Driving fast-spiking cells induces gamma rhythm and controls sensory responses. Nature. 459:663–667.

Carter CS, Mintun M, Cohen JD. 1995. Interference and facilitation effects during selective attention: an H215O PET study of Stroop task performance. Neuroimage. 2:264–272.

Carter CS, van Veen V. 2007. Anterior cingulate cortex and conflict detection: an update of theory and data. Cogn Affect Behav Neurosci. 7:367–379.

Cavanagh JF, Frank MJ. 2014. Frontal theta as a mechanism for cognitive control. Trends Cogn Sci. 18:414–421.

Conner CR, Chen G, Pieters TA, Tandon N. 2014. Category specific spatial dissociations of parallel processes underlying visual naming. Cereb Cortex. 24:2741–2750.

Cox R. 1996. AFNI: software for analysis and visualization of functional magnetic resonance neuroimages. Comput Biomed Res. 29:162–173.

Destrieux C, Fischl B, Dale A, Halgren E. 2010. Automatic parcellation of human cortical gyri and sulci using standard anatomical nomenclature. Neuroimage. 53:1–15.

Egner T, Hirsch J. 2005. The neural correlates and functional integration of cognitive control in a Stroop task. Neuroimage. 24:539–547.

Fischl B. 2012. FreeSurfer. Neuroimage. 62:774–781.

Fischl B, Van Der Kouwe A, Destrieux C, Halgren E, Ségonne F, Salat DH, Busa E, Seidman LJ, Goldstein J, Kennedy D, et al. 2004. Automatically parcellating the human cerebral cortex. Cereb Cortex. 14:11–22.

Flinker A, Chang EF, Kirsch HE, Barbaro NM, Crone NE, Knight RT. 2010. Single-trial speech suppression of auditory cortex activity in humans. J Neurosci. 30:16643–16650.

Ghuman AS, Brunet NM, Li Y, Konecky RO, Pyles JA, Walls SA, Destefino V, Wang W, Richardson RM. 2014. Dynamic encoding of face information in the human fusiform gyrus. Nat Commun. 5:5672.

Gratton G, Coles MG, Donchin E. 1992. Optimizing the use of information: strategic control of activation of responses. J Exp Psychol Gen. 121:480–506.

Kadipasaoglu CM, Baboyan VG, Conner CR, Chen G, Saad ZS, Tandon N. 2014. Surface-based mixed effects multilevel analysis of grouped human electrocorticography. Neuroimage. 101:215–224.

Kadipasaoglu CM, Conner CR, Whaley ML, Baboyan VG, Tandon N. 2016. Category-selectivity in human visual cortex follows cortical topology: a grouped icEEG study. PLoS One. 11:e0157109.

Kerns JG, Cohen JD, MacDonald AW, Cho RY, Stenger VA, Carter CS. 2004. Anterior cingulate conflict monitoring and adjustments in control. Science. 303:1023–1026.

Koga S, Rothermel R, Juhász C, Nagasawa T, Sood S, Asano E. 2011. Electrocorticographic correlates of cognitive control in a stroop task-intracranial recording in epileptic patients. Hum Brain Mapp. 32:1580–1591.

MacDonald AW, Cohen JD, Stenger VA, Carter CS. 2000. Dissociating the role of the dorsolateral prefrontal and anterior cingulate cortex in cognitive control. Science. 288:1835–1838.

Nee DE, Wager TD, Jonides J. 2007. Interference resolution: insights from a meta-analysis of neuroimaging tasks. Cogn Affect Behav Neurosci. 7:1–17.

Oehrn CR, Hanslmayr S, Fell J, Deuker L, Kremers NA, Do Lam AT, Elger CE, Axmacher N. 2014. Neural communication patterns underlying conflict detection, resolution, and adaptation. J Neurosci. 34:10438–10452.

Oldfield RC. 1971. The assessment and analysis of handedness: the Edinburgh inventory. Neuropsychologia. 9:97–113.

Pieters TA, Conner CR, Tandon N. 2013. Recursive grid partitioning on a cortical surface model: an optimized technique for the localization of implanted subdural electrodes. J Neurosurg. 118:1086–1097.

Privman E, Fisch L, Neufeld MY, Kramer U, Kipervasser S, Andelman F, Yeshurun Y. 2011. Antagonistic relationship between gamma power and visual evoked potentials revealed in human visual cortex. Cereb Cortex. 21:616–624.

Privman E, Nir Y, Kramer U, Kipervasser S, Andelman F, Neufeld MY, Mukamel R, Yeshurun Y, Fried I, Malach R. 2007. Enhanced category tuning revealed by intracranial

electroencephalograms in high-order human visual areas. J Neurosci. 27:6234–6242.

Reinhart RMG, Zhu J, Park S, Woodman GF. 2015. Synchronizing theta oscillations with direct-current stimulation strengthens adaptive control in the human brain. Proc Natl Acad Sci USA. 112:9448–9453.

Ridderinkhof KR, Ullsperger M, Crone EA, Nieuwenhuis S. 2004. The role of the medial frontal cortex in cognitive control. Science. 306:443–447.

Saad ZS, Reynolds RC, Argall B, Japee S, Cox RW 2004. SUMA: an interface for surface-based intra- and inter-subject analysis with AFNI. Biomed Imaging Nano to Macro, 2004 IEEE Int Symp. 1510–1513 Vol. 2.

Scherbaum S, Fischer R, Dshemuchadse M, Goschke T. 2011. The dynamics of cognitive control: evidence for within-trial conflict adaptation from frequency-tagged EEG. Psychophysiology. 48:591–600.

Schmidt JR. 2013. Questioning conflict adaptation: proportion congruent and Gratton effects reconsidered. Psychon Bull Rev. 20:615–630.

Shenhav A, Botvinick MM, Cohen JD. 2013. Review the expected value of control: an integrative theory of anterior cingulate cortex function. Neuron. 79:217–240.

Sheth SA, Mian MK, Patel SR, Asaad WF, Williams ZM, Dougherty DD, Bush G, Eskandar EN. 2012. Human dorsal anterior cingulate cortex neurons mediate ongoing behavioural adaptation. Nature. 488:218–221.

Tang H, Yu H-Y, Chou C-C, Crone NE, Madsen JR, Anderson WS, Kreiman G. 2016. Cascade of neural processing orchestrates cognitive control in human frontal cortex. Elife. 5. :Accepted.

Ullsperger M, Bylsma LM, Botvinick MM. 2005. The conflict adaptation effect: it's not just priming. Cogn Affect Behav Neurosci. 5:467–472.

van Steenbergen H, Band GPH. 2013. Pupil dilation in the Simon task as a marker of conflict processing. Front Hum Neurosci. 7:1–11.

van Steenbergen H, Haasnoot E, Bocanegra BR, Berretty EW, Hommel B. 2015. Practice explains abolished behavioural adaptation after human dorsal anterior cingulate cortex lesions. Sci Rep. 5:9721.

Van Veen V, Carter CS. 2005. Separating semantic conflict and response conflict in the Stroop task: a functional MRI study. Neuroimage. 27:497–504.

Venables WN, Smith DM 2008. R Development Core Team. An Introd to R Notes R A Program Environ Data Anal Graph R core team version.

Vidal JR, Ossandón T, Jerbi K, Dalal SS, Minotti L, Ryvlin P, Buschman TJ. 2010. Category-specific visual responses: an intracranial study comparing gamma, beta, alpha, and ERP response selectivity. Front Hum Neurosci. 4:195.

Voytek B, Knight RT. 2015. Dynamic network communication as a unifying neural basis for cognition, development, aging, and disease. Biol Psychiatry. 77:1089–1097.

Whaley ML, Kadipasaoglu CM, Cox SJ, Tandon N. 2016. Modulation of orthographic decoding by frontal cortex. J Neurosci. 36:1173–1184.

Xu M, Xu G, Yang Y. 2016. Neural systems underlying emotional and non-emotional interference processing: an ALE meta-analysis of functional neuroimaging studies. Front Behav Neurosci.. 10:1–15.

Yeung N, Botvinick MM, Cohen JD. 2004. The neural basis of error detection: conflict monitoring and the error-related negativity. Psychol Rev. 111:931–959.

Yeung N, Cohen JD, Botvinick MM. 2011. Errors of interpretation and modeling: a reply to Grinband et al. Neuroimage. 57: 316–319.